International Journal of Robotics and Control Systems
Vol. 6, No. 2, 2026, pp. 1197-1217
ISSN 2775-2658
http://pubs2.ascee.org/index.php/ijrcs

Control-Oriented Steady-State Discharge Modelling of Supercapacitors and Batteries for Closed-Loop BLDC Motor Systems Using ARX and ARMAX Model

Azri A. Aziz [a,1,*], M. Saifizi Saidon [a,2,*], Siti Marhainis Othman [a,3], M. Izuan Fahmi Romli [a,4], Muhammad Abdullah [b,5]

[a] Faculty of Electrical Engineering & Technology, Universiti Malaysia Perlis, 02600 Arau, Perlis, Malaysia
[b] Department of Mechanical and Aerospace Engineering, International Islamic University Malaysia, 53100 Kuala Lumpur, Malaysia
[1] azriaziz@unimap.edu.my; [2] saifizi@unimap.edu.my; [3] marhainis@unimap.edu.my; [4] izuanfahmi@unimap.edu.my; [5] mohd_abdl@iium.edu.my
* Corresponding Author

ARTICLE INFO

Article history
Received November 20, 2025
Revised January 14, 2026
Accepted April 19, 2026

Keywords
ARX and ARMAX Model;
Steady-State Discharge;
Close-Loop System;
Supercapacitor Battery;
BLDC Motor

ABSTRACT

This paper investigates control-oriented steady-state discharge modelling of a supercapacitor (SC) and a lithium-ion battery supplying a brushless DC (BLDC) motor in a closed-loop system. The study addresses the lack of discharge models that represent energy storage behavior under motor loading conditions, which is critical for accurate current regulation in electric vehicle applications. Linear black-box identification using ARX and ARMAX structures is employed to model the relationship between PWM duty cycle and discharge current at fixed operating points. Experimental data are collected from a laboratory-scale BLDC drive with a sampling time of 0.01 s, focusing on steady-state operation at reference currents of 0.4 A and 0.6 A. System identification is performed using segmented datasets, and model orders are selected through a guided process that prioritizes low computational complexity while maximizing best-fit accuracy. Model performance is evaluated using prediction best-fit metrics. Results show that ARMAX models consistently outperform ARX models, achieving best-fit values of up to 91.96% for the SC and 89.84% for the battery, representing an improvement of approximately 3%. This improvement indicates enhanced prediction accuracy and disturbance handling, which directly supports smoother and more reliable closed-loop current control. The research contributes a validated modelling framework for EV energy storage systems that enables accurate current estimation and improved control efficiency.

1. Introduction

The continuous advancement of electric vehicle (EV) technologies is transforming modern transportation by replacing conventional internal combustion engines with electrically driven propulsion systems. Among the various motor types developed for EV applications, the Brushless Direct Current (BLDC) motor has emerged as a leading candidate owing to its compact design, high

efficiency, and favorable torque-speed characteristics as mention in [1]-[3]. In EV powertrain design, the configuration of the drive system and motor control strategy plays a pivotal role in achieving high energy efficiency and optimal vehicle performance. The BLDC motor offers several advantages, including robust torque generation, wide speed range, high power density, and increased reliability under variable operating conditions [4]-[6]. This study investigates the BLDC motor operation powered by SC and battery as the energy source. The evaluation of discharge behavior involves current response characteristic and suitability for controlled operation.

Maintaining system stability under fluctuating load and speed conditions remains one of the primary challenges in BLDC based EV applications. Disturbances such as voltage oscillations and current ripple can degrade both energy efficiency and mechanical response [7], [8]. These issues become especially prominent in non-sinusoidal BLDC systems operating within field-weakening regions, where advanced control and power management strategies are essential to maintain smooth torque output. To mitigate these effects, modern EV architectures incorporate buck/boost DC-DC converters that regulate power exchange among the lithium-ion battery, the ESS, and the motor during both motoring and regenerative braking modes as mention in many research [9]-[12]. This arrangement enables seamless mode switching between acceleration and energy recovery, thereby enhancing system efficiency. Previous studies have also highlighted that supercapacitors (SCs)-based regenerative braking significantly reduces energy losses while improving torque response and drive smoothness [13], [14]. Comparing SCs and batteries helps identify suitable energy storage configurations for different motor operating conditions, especially during high acceleration and regenerative braking [15].

Recent reviews of EV propulsion technologies emphasize the importance of precise BLDC motor speed control under both steady-state and dynamic conditions [16]. In this context, accurate modeling of the ESS discharge characteristics is fundamental to developing effective control algorithms. A well-identified system model not only captures the system's dynamic response but also improves controller tuning and performance evaluation under steady-state operation. Steady-state condition where the system in stable operation required several approaches mainly examine electrical or mechanical quantities particularly in BLDC motor, where the stable operating region allows clearer observation of torque production, current behavior, and speed regulation [17]. In this condition, different analysis techniques are applied to achieve more accurate evaluation and reliable performance assessment in these two conditions steady-state and dynamic-state [18], [19]. Linear model structures such as Auto-Regressive with Exogenous Input (ARX) and Auto-Regressive Moving Average with Exogenous Input (ARMAX) have proven effective in capturing the input/output dynamics of energy storage systems (ESS) operating under closed-loop control [20]. Their computational efficiency and robustness against disturbances make them particularly suitable for real-time implementation in embedded systems [21], [22]. The ARX model is typically applied to systems that are dynamic and require frequent updates and feedback, its relatively simple structure makes it suitable for such applications [23], [24]. While, ARMAX model suitable for multi-input computational [25]. ARX model imposes a low computational burden, cost effective and real-time estimation making it feasible to integrate with other methods [26]-[28]. Researchers [29] state that ARX and ARMAX model capable of accurately, particularly when aiming to obtain the simplest model possible to optimize computational resources.

Existing energy storage modelling approaches for electric vehicle applications mainly focus on battery or SC self-discharge characteristics, long-term degradation, or electrochemical behavior under static conditions. While these models provide insight into internal storage properties, it does not adequately represent discharge behavior when the energy storage system actively supplies power to an electric motor, particularly under closed-loop control conditions. Closed-loop systems provide improved control accuracy by continuously correcting the output and adapting to operational changes, ensuring stable and reliable performance for real-time applications despite increased complexity [30]-[32]. In process control systems where accuracy is prioritized, closed-loop control minimizes tracking error and enhances system stability through feedback-based correction and maintain stable

performance [33], [34]. The closed-loop structure provides a stable and effective foundation for basic control, enabling higher-level or advanced control strategies to operate dependably [35].

In electric vehicles, efficient battery management depends heavily on accurate and rapid estimation of the State of Charge (SOC) [36], [37]. To enhance SOC prediction accuracy for lithium-ion batteries, researchers have explored various adaptive estimation algorithms. For instance, the study in [38] proposed a recursive least squares (RLS) approach with a variable forgetting factor, improving estimation precision under varying load conditions. Maintaining a low charge rate is also vital to mitigate thermal stress and prevent capacity degradation, as excessive heat accelerates battery aging. Achieving an optimal balance between fast charging and battery longevity remains a persistent engineering challenge. In this regard, the work in [39] demonstrated that combining two distinct charging techniques can shorten charging duration without significantly reducing battery lifespan. Recent research [40], [41] introduced a hybrid energy storage configuration that integrates batteries with SCs to enhance overall performance and extend the operational lifespan of battery energy storage systems (BESS), while it can improve the driving range in term of EV application [42]. The inclusion of SCs effectively reduces the stress on battery cells during high-power demand or transient load events [43]. Furthermore, advances in nonlinear system identification techniques have been applied to improve the safety, performance, and durability of both Li-ion batteries and SCs [44], [45]. These approaches provide more accurate energy characterization, supporting smarter energy management and improved reliability under dynamic load conditions.

SCs exhibit high capacitance, long cycle life, and excellent power density, making them ideal for backup, pulse, and hybrid energy applications. Recent innovations [46] have incorporated SCs as auxiliary energy sources in hybrid energy storage systems (HESS), particularly alongside proton-exchange membrane fuel cells (PEMFCs), improving system adaptability and transient response. The integration of SCs enables rapid power delivery, enhancing both efficiency and stability during high-demand operation. Researchers in [47], [48] combined multiple energy source as hybrid system such as wind turbine, batteries and SC. Alongside with advanced control and power conversion techniques which aim to enhance energy reliability, efficiency, and system performance by coordinating diverse sources. The integration of SCs within the energy storage system (ESS) further enhances overall drivetrain performance by improving transient response and energy utilization efficiency [49]-[51]. Such hybrid configurations facilitate energy recovery during braking events and redistribute stored energy to support acceleration phases. Nevertheless, torque ripple, transient current variations, and speed fluctuations often arise in these systems, occasionally leading to performance inconsistencies [52].

In BLDC motor-driven systems, the discharge current is strongly influenced by motor dynamics, converter switching, and control actions. Models developed for self-discharge or open-circuit conditions fail to capture these interactions, leading to inaccurate current prediction and limited applicability for control design. Furthermore, physics-based models require extensive parameterization and are difficult to adapt for real-time control implementation, especially when operating at specific motor speeds. The present study focuses on a comparative analysis of SC and battery discharge characteristics under closed-loop control. By applying ARX and ARMAX modeling techniques, this research aims to identify and characterize system performance in steady-state operation and evaluate model accuracy using best-fit criteria. Experimental validation is performed through a hardware platform that emulates an EV motor drive, with control inputs and feedback signals managed via Simulink interfacing. Unlike physics-based electrochemical models, which require extensive parameterization and are difficult to adapt for real-time control, black-box ARX/ARMAX models offer a control-oriented and computationally efficient alternative for steady-state operation. This work contributes toward improved ESS modeling for electrical mobility applications by offering reliable prediction tools in real-time energy management to improve control efficiency and operational reliability. Although ARX and ARMAX models have seen widespread use in control system identification, few have questioned their relevance to the modeling of SC and battery discharge during closed-loop steady-state operation of BLDC motors. The available models cover

mostly dynamic or transient regimes. This paper therefore addresses this gap by suggesting and validating ARX and ARMAX models of steady-state discharge behavior. The manuscript is organized into four main sections: Introduction, Research Method, Results, Discussion and Conclusions.

2. Research Method

2.1. Experiment Setup and Research Design

The experimental setup features a BLDC motor system powered by a 188 F, 51-volt SC and 48-volt battery connected to a 500-watt, 48-volt BLDC motor via a 48-volt DC-DC converter. This setup is utilized to study and validate the battery and SC's discharge behavior and the motor's performance. The hardware system is designed to simulate a real BLDC motor in a scooter, with a standard wheel attached for authentic load operation. Fig. 1 illustrates the experimental configuration in which SC and battery are employed as power source to drive a BLDC motor, serving as the system load. A current sensor ACS712 rated 5-A was utilized to monitor the discharge behavior of the hybrid power sources, while MATLAB/Simulink interfaced with the Digital Signal Processor (DSP) Launchxl-F28379D to execute signal processing and control tasks. As shown in Fig. 2, the hardware configuration represents a laboratory-scale prototype of an electric scooter, replicating the BLDC motor load while allowing flexible data collection and parameter adjustment. Several hardware modifications were made to ensure reliable communication between the DSP microcontroller and the input manipulation circuitry, thereby maintaining signal accuracy and system responsiveness throughout the tests.

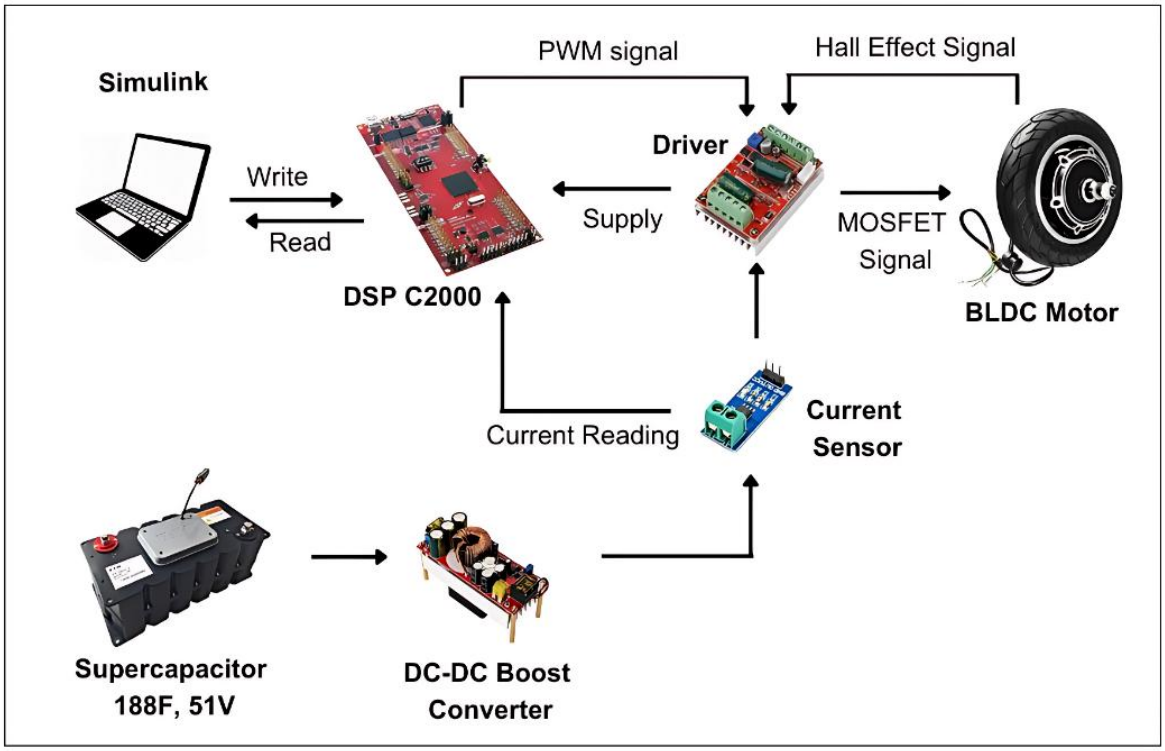

Fig. 1. Flow of experiment setup with power sources

The overall experimental framework, shown in Fig. 3, was organized into three main phases: (i) development of the experimental platform, (ii) identification of the system model, and (iii) validation and analysis of system performance. The flowchart outlines the procedure for developing a closed-loop SC and battery discharge model for BLDC motor operation. A preliminary tests to establish the current-PWM relationship. Linear modelling is then applied and evaluated in a closed-loop framework, followed by steady-state verification through PWM adjustment. Once stable operation is achieved, the discharge model is designed and analyzed using validated input-output data.

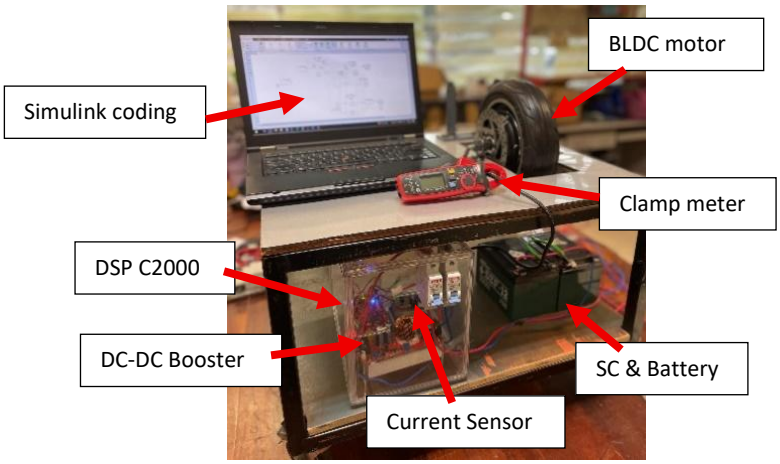

Fig. 2. Experimental hardware setup

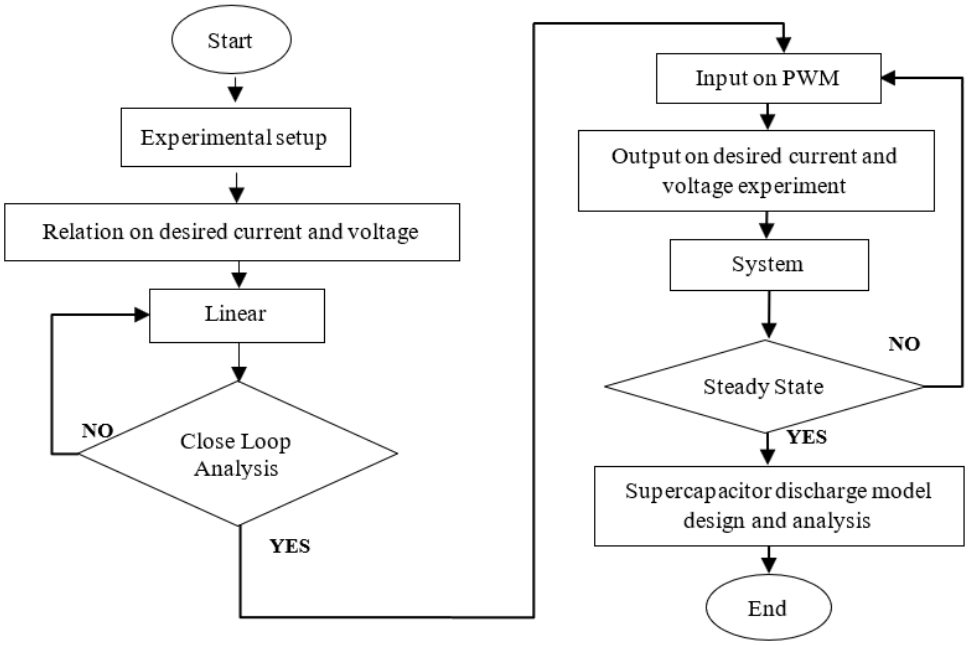

Fig. 3. Block diagram of research design

The control of BLDC motor speed primarily depends on the manipulation of Pulse Width Modulation (PWM) signals generated within the DSP controller [53], [54]. To evaluate performance, various duty cycle values were applied to observe motor response across a range of speeds. Although the battery offers a more stable energy output than the SC, a DC-DC boost converter was integrated into the battery line to maintain a consistent 48 V output [55]. The current supplied to the BLDC motor driver originating either from the battery or the SC is continuously monitored using the ACS712 current sensor [56], This sensor was calibrated to ensure that the floating current value corresponded closely with multimeter measurements, thereby improving accuracy. Because the analog sensor readings are often noisy or ambiguous, the signal must be converted into a digital form interpretable by the DSP. A key consideration in this process is the offset current value, which is determined according to the expression provided in Equation (1),

$$Float\ Current\ (i) = \frac{Offset\ reading - analogue\ reading}{*\boldsymbol{Sensitivity}} \quad (1)$$

Current sensor ***Sensitivity*** for ACS712/05BT = 185 [57].

2.2. Closed-Loop System Setup

In this experiment, a closed-loop control configuration was employed to obtain discharge current profiles and PWM input data for both the battery and the SC. All tests were conducted with a sampling time of 0.01 seconds to ensure adequate temporal resolution. The dominant current dynamics of the closed-loop BLDC system were observed to lie below 20 Hz based on the measured rise and settling times. Therefore, a sampling rate of 100 Hz satisfies the Nyquist criterion for control-oriented system identification. High-frequency switching effects were attenuated through digital filtering prior to model identification. Fig. 4 illustrates the Simulink model used in the setup, which interfaces with the hardware through a real-time controller for instruction transfer and data acquisition. The implementation integrates MATLAB/Simulink with the Texas Instruments (TI) C2000 platform, allowing program execution within the Digital Signal Processor (DSP) environment. In the control framework, Simulink generates PWM signals that act as input commands to the ePWM module, while the Analog-to-Digital Converter (ADC) module simultaneously records current feedback from the energy storage unit. After signal conditioning through a digital filtering process, the processed current feedback is transmitted back to the controller input, thereby completing the closed-loop regulation cycle.

For example, when a reference input current of 0.4 A is specified, it is continuously compared with the measured feedback current. The ePWM module then adjusts the duty cycle to produce the appropriate PWM signal, ensuring that the BLDC motor operates at the corresponding target speed. This operating speed directly defines the current demand from the power source. On the output side, the ADC module captures the current readings from the ACS712 sensor and converts them into floating-point values, as represented in Equation (1). The measured data are subsequently filtered in discrete form and fed back into the control loop, ensuring stable and accurate closed-loop operation throughout the experiment.

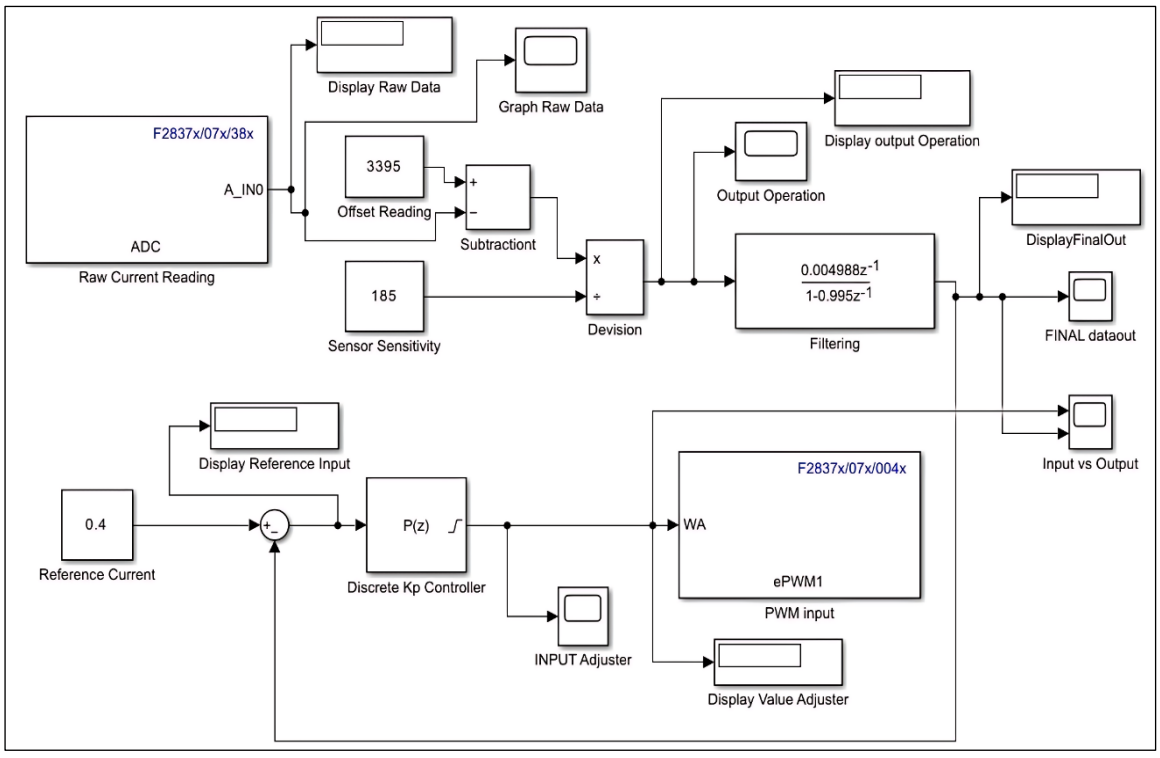

Fig. 4. Simulink design close loop system

2.3. Linear Polynomial ARX and ARMAX Analysis

The operation of a BLDC motor can generally be classified into two distinct conditions, steady-state and dynamic-state operation, which together define the motor's overall performance

characteristics [58]. Under steady state, constant speed and torque improve efficiency and energy lifespan, while dynamic state analysis evaluates transient responses crucial for robust control and system stability [59]. This study focuses on steady-state experiments to accurately characterize motor electrical and mechanical parameters under controlled, repeatable conditions.

ARX and ARMAX models are commonly employed to analyze and predict the static and dynamic behavior of control systems. These models align input and output data to facilitate accurate system identification, enabling researchers to capture the system's transient and steady-state responses for subsequent validation and performance evaluation. The black-box approach is employed to identify systems based solely on input and output data. With no prior knowledge of the system's internal dynamics, various combinations of poles and zeros were tested to determine the configuration that achieved the highest best-fit to the system. Experimental input-output data is used for system identification, estimating the system's response. Polynomials are fitted to represent the numerator and denominator of the transfer function, generating the discrete-time model $G(z)$ that links input $U(z)$ to output $Y(z)$. The transfer function from ARX or ARMAX is directly interpreted as:

$$G(z) = \frac{Output\ polynomial}{Input\ polynomial} \tag{2}$$

The z-transform is used to represent the system in the discrete-time domain, where the z^{-1} operator denotes one-sample delay. The ARMAX model extends ARX Equation (3) by incorporating a moving average (MA) term to account for noise dynamics Equation (4). Both equations can be converted into the z-domain to obtain the discrete-time transfer function, represented as:

$$\frac{Y(z)}{U(z)} = \frac{b_1 z^{-1} + b_2 z^{-2} + \cdots + b_m z^{-m}}{1 + a_1 z^{-1} + a_2 z^{-2} + \cdots + a_n z^{-n}} \tag{3}$$

$$H(z) = \frac{1 + c_1 z^{-1} + c_2 z^{-2} + \cdots + c_k z^{-k}}{1 + a_1 z^{-1} + a_2 z^{-2} + \cdots + a_n z^{-n}} \tag{4}$$

Where, $(Y(z))/(U(z))$ represents the transfer function $G(z)$, a, b and c represent the input, output and noise value. While, ARMAX provides a noise model $H(z)$ to describe how disturbances influence the system. The System Identification Toolbox efficiently estimates coefficients for both $G(z)$ (system dynamics) and $H(z)$ (noise dynamics), enabling comprehensive system modeling. Whereas, input variable inside system identification MATLAB, value of [na], [nb], [nc] for moving average and [nk] for error terms determine the order of transfer function and this value are being tested to obtain the highest best-fit to the system identification toolbox.

3. Results and Discussion

In the closed-loop system, current feedback acquisition, regulated by proportional control (Kp) [60], adjusts the input to achieve target output currents. Reference currents of 0.4 A and 0.6 A were selected to evaluate PWM responses under low and high-speed conditions. At idle, where the BLDC motor operates without load, the maximum current is approximately 1.0 A. Several tests with repeatability were conducted to identify suitable values, with 0.4 A representing lower speeds and 0.6 A higher speeds, ensuring stable and reliable readings. Fig. 5 shows the battery's PWM input for 0.4 A, where duty cycle reaches around 80% to maintain output. Fig. 6 demonstrates the PWM input for 0.6 A increased fluctuations in output current, demanding a maximum 100% duty cycle.

For the SC, at Fig. 7, when a reference current of 0.4 A is applied, the measured output current fluctuates between approximately between 0.37 A and 0.47 A. But there are certain spikes reaching 0.49 A indicate that unstable burst of current. The corresponding PWM input varies from 0% up to an average duty cycle of around 85% and at current 0.49 A shows 100% duty cycle. This variation reflects the SC's rapid charge/discharge characteristics and its limited capacity to sustain a constant output under load conditions. For a 0.6 A reference shown in Fig. 8, output current fluctuates from 0.55 A to 0.67 A, and PWM input peaks from 0% to 100% duty cycle, indicating a greater adjustment

requirement for maintaining output stability at higher current settings. Hence, 0.6 A reference current yield the 100% duty cycle represent the high speed of motor operation.

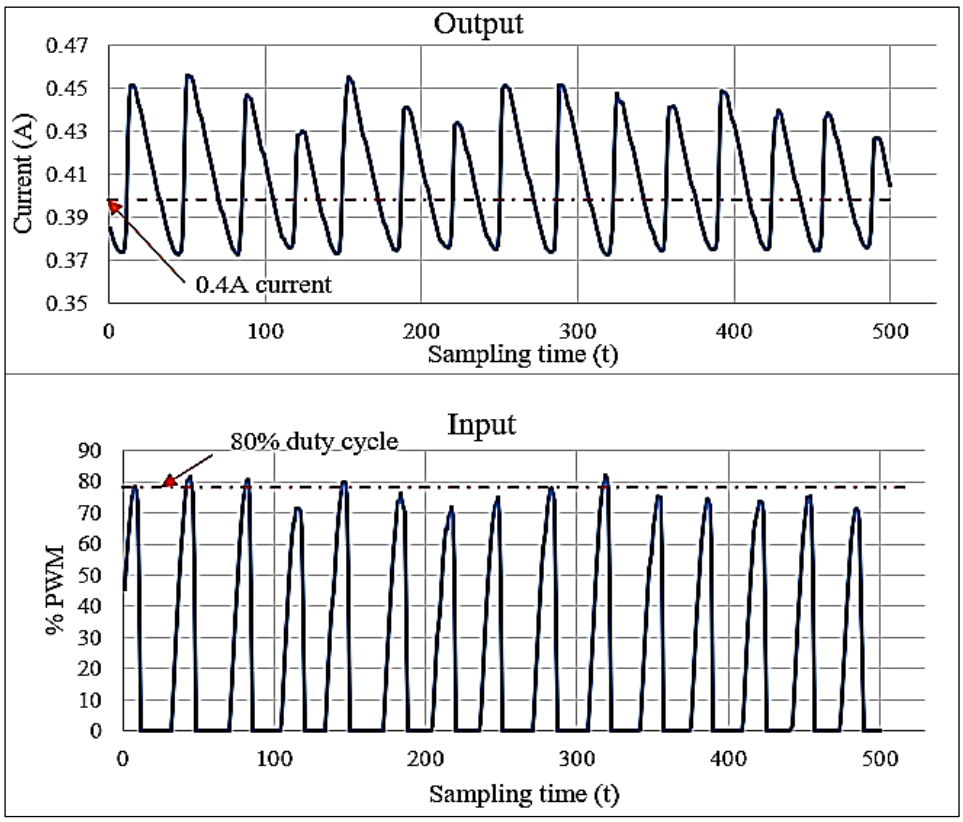

Fig. 5. Battery's PWM input for 0.4 A current

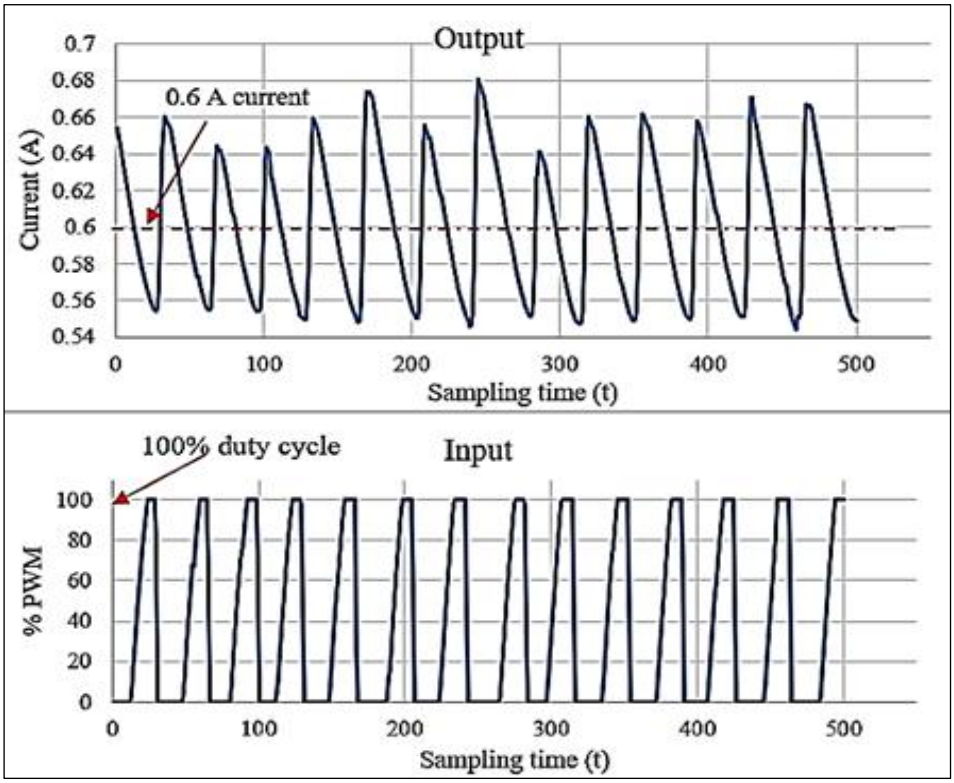

Fig. 6. Battery's PWM input for 0.6 A current

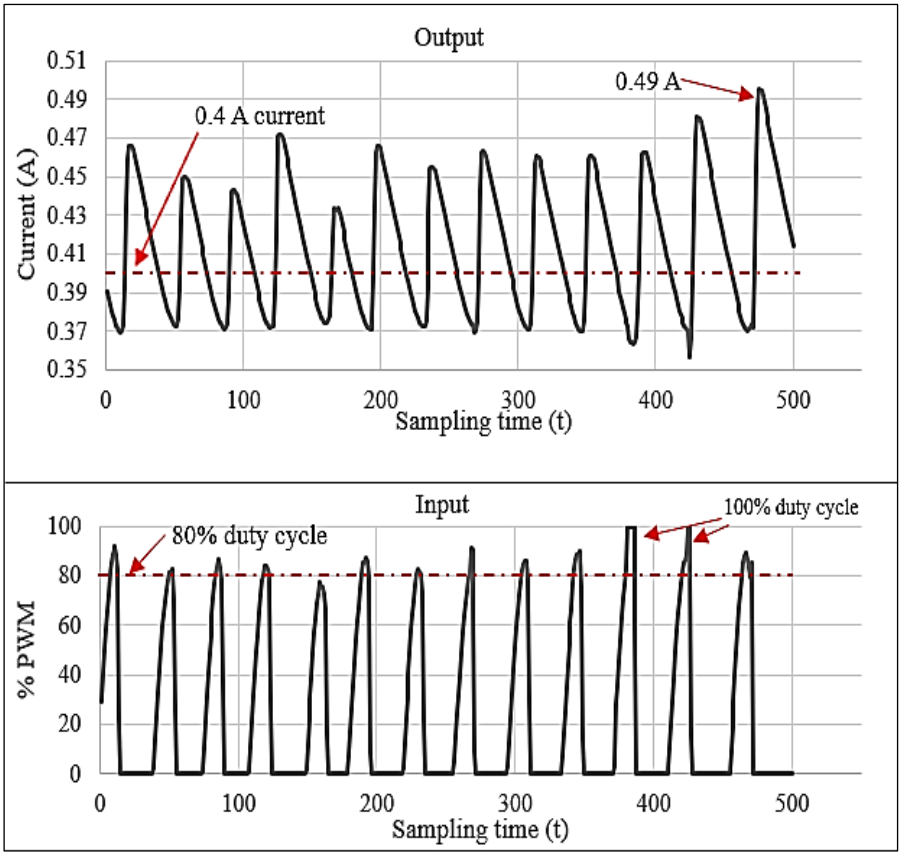

Fig. 7. SC's PWM input for 0.4 A current

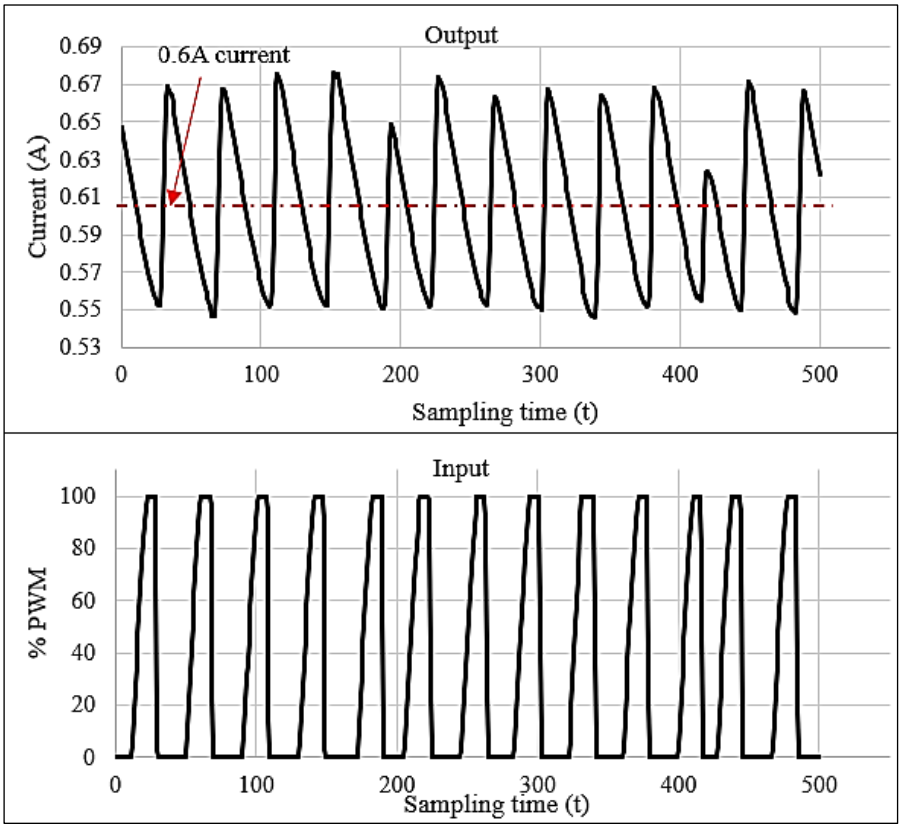

Fig. 8. SC's PWM input for 0.6 A current

3.1. Battery Close-Loop ARX and ARMAX Analysis

The closed-loop analysis compares battery and SC discharge characteristics using ARX and ARMAX models. Batteries, with higher energy density but lower power density than SCs, deliver smoother output with minor current fluctuations. Table 1 demonstrates the ARX and ARMAX model applied to battery discharge currents for 0.4 A and 0.6 A reference values, achieving best-fit percentages of **89.11%** and **85.06%,** respectively, using ARX structures [10 9 1] and [10 10 1]. While, for ARMAX with the delay parameter [nk] set to 1, [na nb nc nk] represents the ARMAX order. Repeated tests of different orders showed that higher orders produce better best-fit results such as order [10 8 8 1] achieved a **91.96%** best-fit for the 0.4 A reference-current and **90.84%** best-fit for the 0.6 A reference-current using 100-sample data. The selection of ARX and ARMAX model orders was performed using a guided and systematic procedure rather than arbitrary trial-and-error. Model identification started with low-order structures to maintain computational efficiency and suitability for closed-loop control. The orders were then gradually increased, and each candidate model was evaluated based on prediction best-fit accuracy and residual behavior. The order selection was constrained by two main criteria. First, lower-order models were prioritized to reduce computational burden and to maintain suitability for real-time control implementation. Second, the model providing the highest best-fit accuracy to the measured output was selected. This approach ensures a balanced trade-off between model simplicity and prediction accuracy. By progressively increasing the model order within these constraints, the selected ARX and ARMAX configurations were able to achieve reliable representation of the discharge behavior without unnecessary model complexity.

Fig. 9 and Fig. 10 present measured vs. simulated ARX. While, Fig. 11 and Fig. 12 present ARMAX model outputs for the respective current references, highlighting the steady state response differences between battery models. The discrete-time model was sampled at 0.01 second intervals, producing an experimental dataset of roughly 8,000 data points, equivalent to a sampling frequency of 100 Hz. Each 100-point segment therefore represents one second of data, which was found to be adequate for capturing the system's dynamic behavior without excessive redundancy. While higher sampling rates may capture switching-level dynamics, the objective of this study is control-oriented steady-state discharge modelling. Therefore, the selected sampling rate prioritizes relevant system dynamics rather than high-frequency switching behavior. To investigate the influence of dataset size, larger windows containing 300-data and 500-data points were also evaluated shown in Table 1. 300-sample data and 500-sample data are not performed as 100-sample data testing. Interestingly, the results showed that using 100-data points yielded the highest model fit accuracy. Increasing the dataset size beyond this threshold did not enhance the model's predictive performance and, in some cases, introduced unnecessary computational overhead due to redundant information. The ability of high accuracy prediction of steady-state discharge makes smooth current sharing between SC and battery possible using effective energy management policies in EVs, enhancing the reliability of the system.

Table 1. ARX and ARMAX close-loop analysis for Battery

Reference Current (A)	Number of Sample Data Testing	Polynomial ARX order structure [na nb nk]	ARX Percentage of Best-Fits (%)	Polynomial ARMAX order structure [na nb nc nk]	ARMAX Percentage of Best-Fits (%)
0.4	**100**	[10 9 1]	**89.11**	[10 8 8 1]	**91.96**
	300		82.74		88.85
	500		64.00		72.07
0.6	**100**	[10 10 1]	**85.06**	[10 8 8 1]	**90.84**
	300		76.19		78.88
	500		50.95		64.02

The best-fit value is used to evaluate how well the developed mathematical model represents the actual system output. It compares the model-predicted output current with the measured discharge current obtained from the experiment. A higher best-fit percentage indicates that the model output closely follows the real system behavior, while a lower value indicates larger prediction errors. In this

study, the best-fit result is calculated based on the difference between the measured current and the current estimated by the ARX or ARMAX model over the same data segment. The value reflects the model's ability to capture the dominant discharge dynamics of the energy storage system supplying the BLDC motor under steady-state conditions. Models with higher best-fit values are considered more accurate and reliable for representing the discharge behavior at the selected operating point.

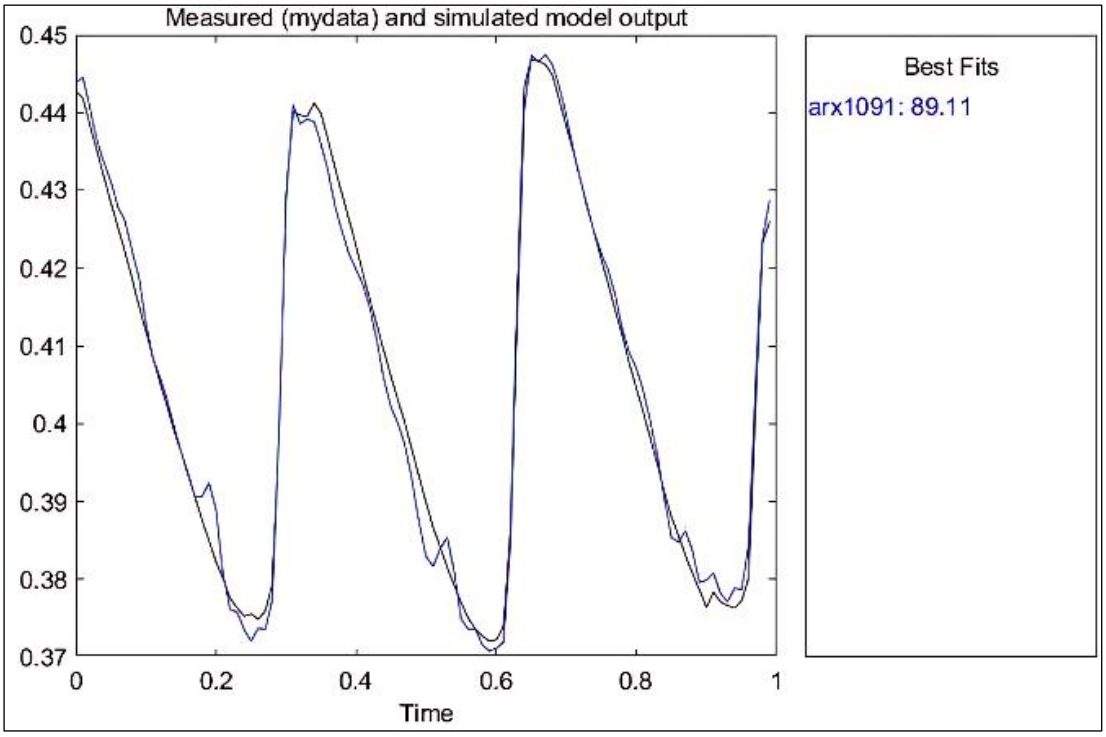

Fig. 9. Best-fit for battery's ARX model outputs 0.4 A

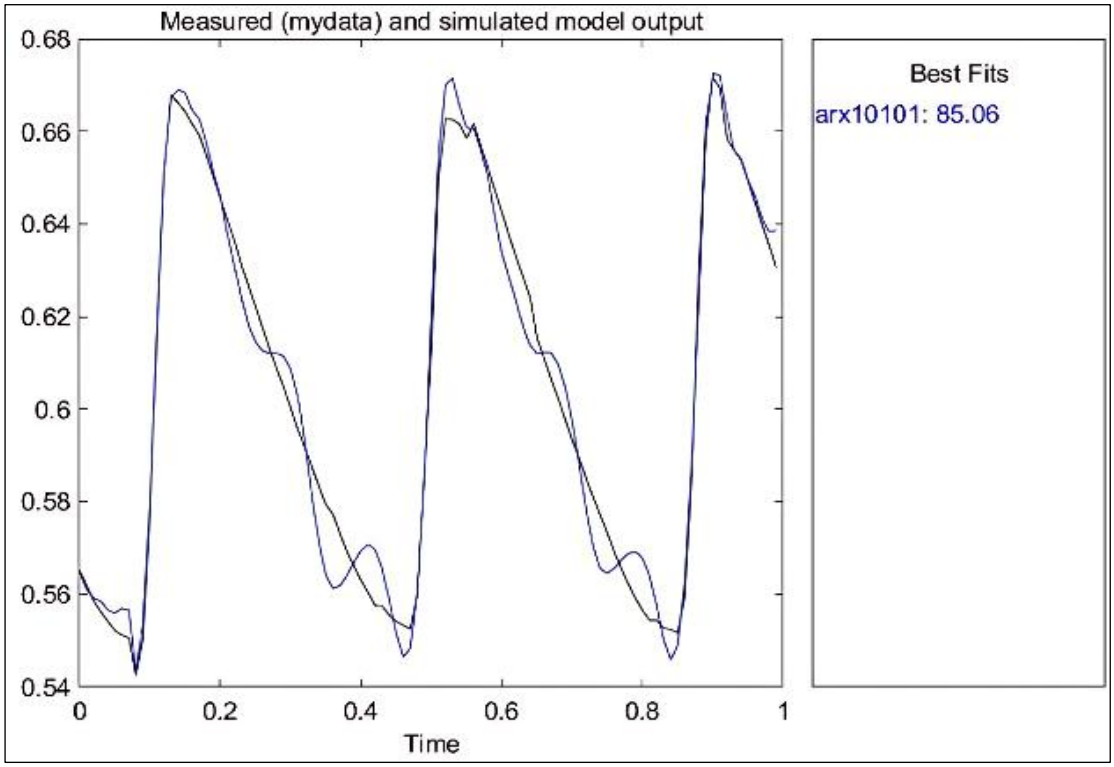

Fig. 10. Best-fit for battery's ARX model outputs 0.6 A

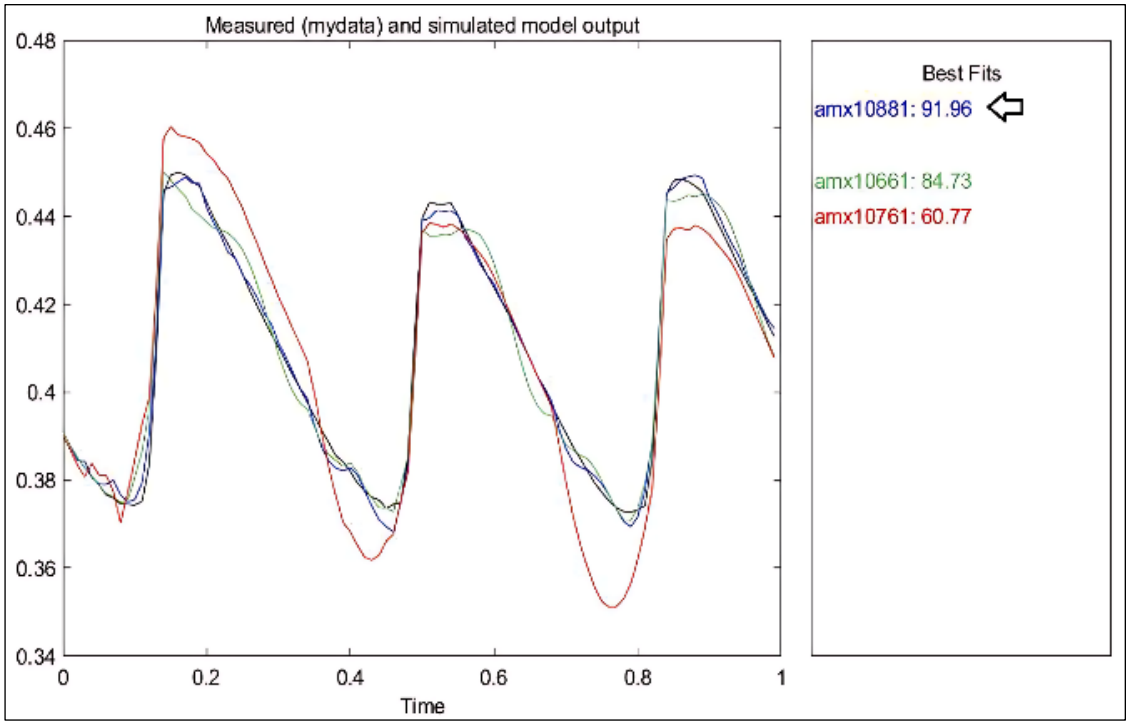

Fig. 11. Best-fit for battery's ARMAX model outputs 0.4 A

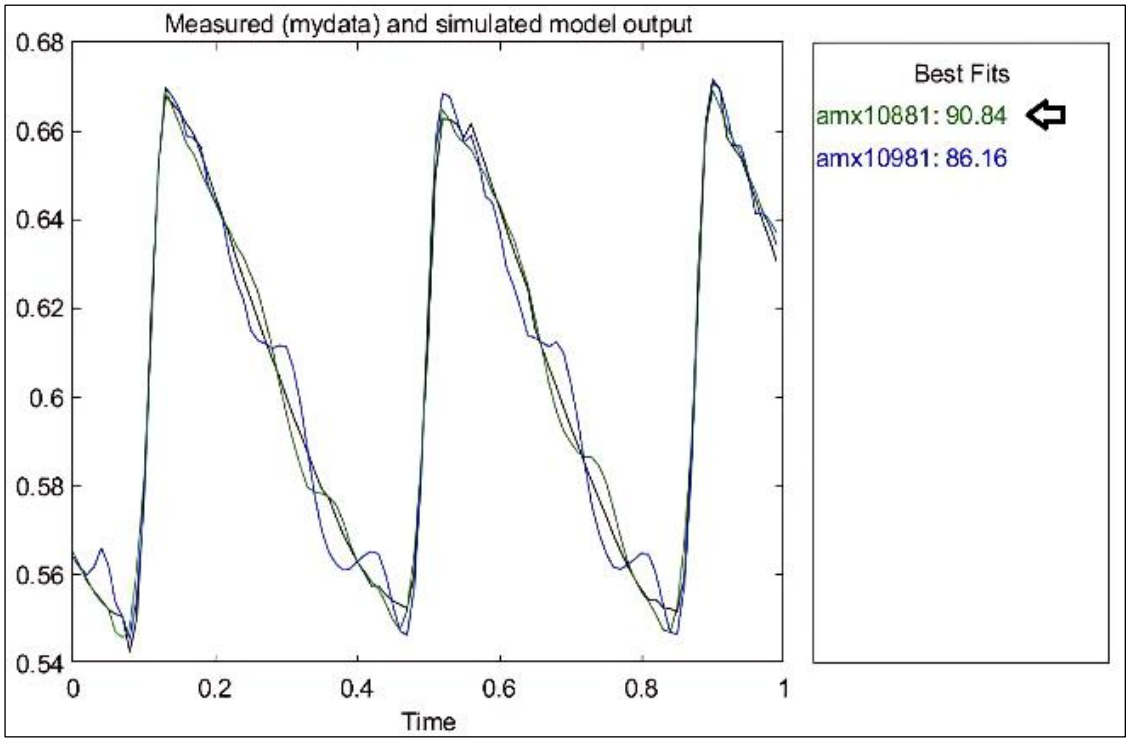

Fig. 12. Best-fit for battery's ARMAX model outputs 0.6 A

3.2. Supercapacitor (SC) Close-Loop ARX and ARMAX Analysis

For SCs, Table 2 shows best-fit percentages of **82.42%** for a 0.4 A reference current and **86.26%** for a 0.6 A reference current with a [10 10 1] polynomial ARX structure, achieved using the same setup as the battery analysis. While, polynomial ARMAX model for SC analysis, covering two reference currents, 0.4 A and 0.6 A. The ARMAX order [9 6 6 1] achieved the highest best-fit values

of **89.84%** for 0.4 A and **89.53%** for 0.6 A within 100-sample datasets. Additional tests were performed using 300-sample and 500-sample datasets, and the outcomes exhibited behavior consistent with the battery's response. Same as dataset in battery, 300-dataset and 500 data-set also not suitable as results shown lower best-fit value.

Table 2. ARX and ARMAX close-loop analysis for SC

Reference Current (A)	Number of Sample Data Testing	Polynomial ARX order structure [na nb nk]	ARX Percentage of Best-Fits (%)	Polynomial ARMAX order structure [na nb nc nk]	ARMAX Percentage of Best-Fits (%)
0.4	**100**	[10 10 1]	**82.42**	[9 6 6 1]	**89.84**
	300		83.16		86.27
	500		72.03		79.66
0.6	100	[10 10 1]	**86.26**	[9 6 6 1]	**89.53**
	300		79.12		80.69
	500		68.93		76.08

Fig. 13 and Fig. 14 compare the measured discharge current from the experiment with the current predicted by the developed ARX model. In both figures, the measured current represents the actual behavior of the SC supplying the BLDC motor, while the simulated output represents the response generated by the mathematical model using the same input signal. In Fig. 13, the ARX model achieves a best-fit value of 82.42% at reference current 0.4 A. This means that the model is able to reproduce most of the measured current trend, including the general rise and fall pattern of the discharge current over time. However, small differences can still be observed, especially at the peak and valley regions, indicating that some dynamic effects are not fully captured by the model. In Fig. 14, the ARX model shows an improved best-fit value of 86.26% at reference current 0.6 A. The simulated output follows the measured current more closely, particularly during transitions between higher and lower current levels. This higher best-fit value indicates better agreement between the model and the real system, meaning the model can predict the discharge behavior more accurately at this operating condition. In contrast, prior work [61] focused on supercapacitor self-discharge modeling in simulation, whereas this study experimental models the complete discharge process driving a BLDC motor.

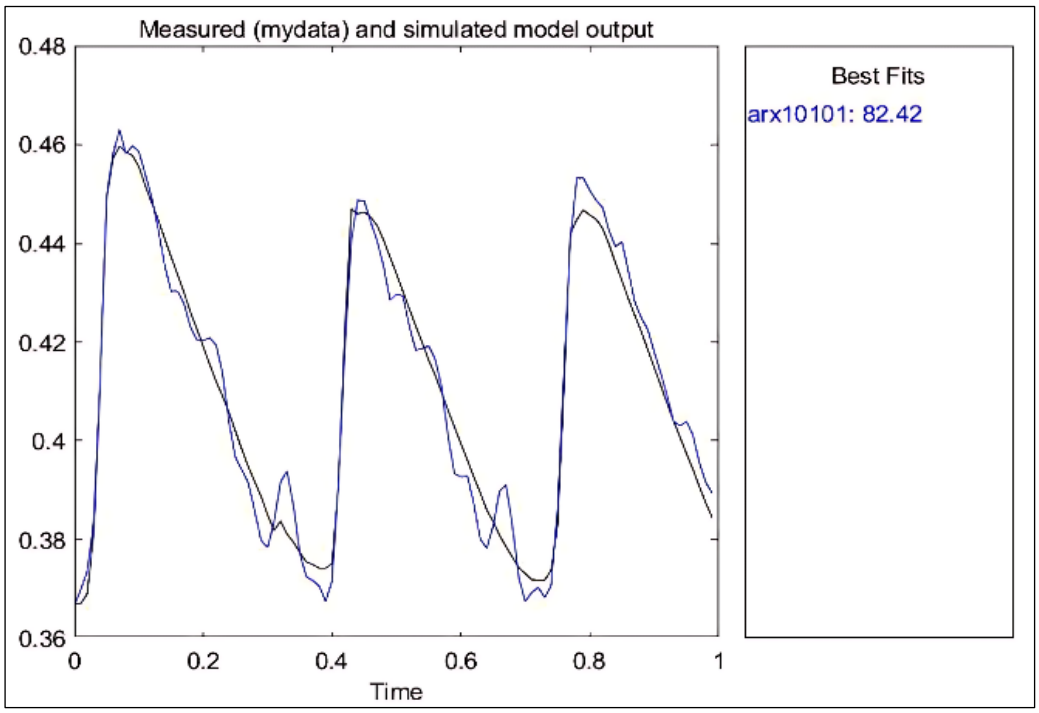

Fig. 13. Best-fit for SC's ARX model outputs 0.4 A

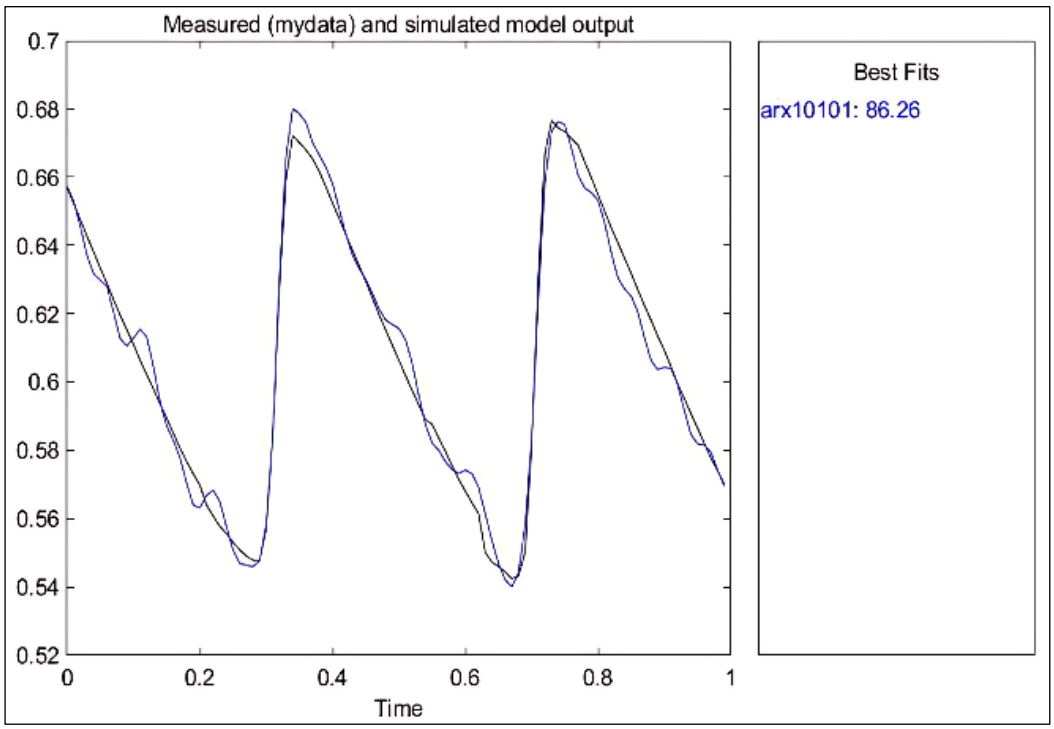

Fig. 14. Best-fit for SC's ARX model outputs 0.6 A

Meanwhile, Fig. 15 and Fig. 16 present the simulated outputs of the ARMAX model for the SC discharge, with best-fit values of 89.84% and 89.53%, respectively. Compared with the ARX results, these values indicate a clear improvement in model accuracy. The ARMAX model output follows the measured discharge current more closely over the entire operating period, particularly during transition regions where small fluctuations and disturbances occur. This improvement is mainly due to the inclusion of the moving average component in the ARMAX structure, which allows the model to account for measurement noise and unmodelled dynamics more effectively. As a result, the predicted current signal shows reduced deviation from the experimental data, especially near current peaks and during gradual decay regions.

Table 3 summarizes the best-fit result with order for both battery and SC, while Table 4 and Table 5 list the mathematical modeling with specific parameters detail according to experimental reference current.

Table 3. Summary of ARX and ARMAX close-loop analysis for battery and SC

Energy System	Reference Current (A)	Model	Order [na nb nc nk]	Best-Fit (%)
Battery	0.4	ARX	[10 9 1]	89.11
Battery	0.4	ARMAX	[10 8 8 1]	**91.96**
Battery	0.6	ARX	[10 10 1]	85.06
Battery	0.6	ARMAX	[10 8 8 1]	**90.84**
SC	0.4	ARX	[10 10 1]	82.42
SC	0.4	ARMAX	[9 6 6 1]	**89.84**
SC	0.6	ARX	[10 10 1]	86.26
SC	0.6	ARMAX	[9 6 6 1]	**89.53**

Table 4 shows discrete-time ARX equations for comparing battery and SC discharge, whereas Table 5 compared ARMAX model orders with their highest best-fit. For ARX model, battery analysis shows 0.4 A reference current give the highest best-fit 89.11%, while for SC, 0.6 A reference current shows highest best-fit 86.26%. Then, for ARMAX model, both battery and SC represent by 0.4 A reference current for highest best-fit 91.96% and 89.84% respectively. The greater precision of the ARMAX model (2–3% improved best-fit) confirms that the ability to better observe noise dynamics

is a requirement in real-time EV control systems where feedback signals are always noisy. Although the numerical improvement in best-fit is approximately 3%, this enhancement significantly improves current prediction accuracy, resulting in smoother duty-cycle adjustment and reduced steady-state oscillations in closed-loop operation.

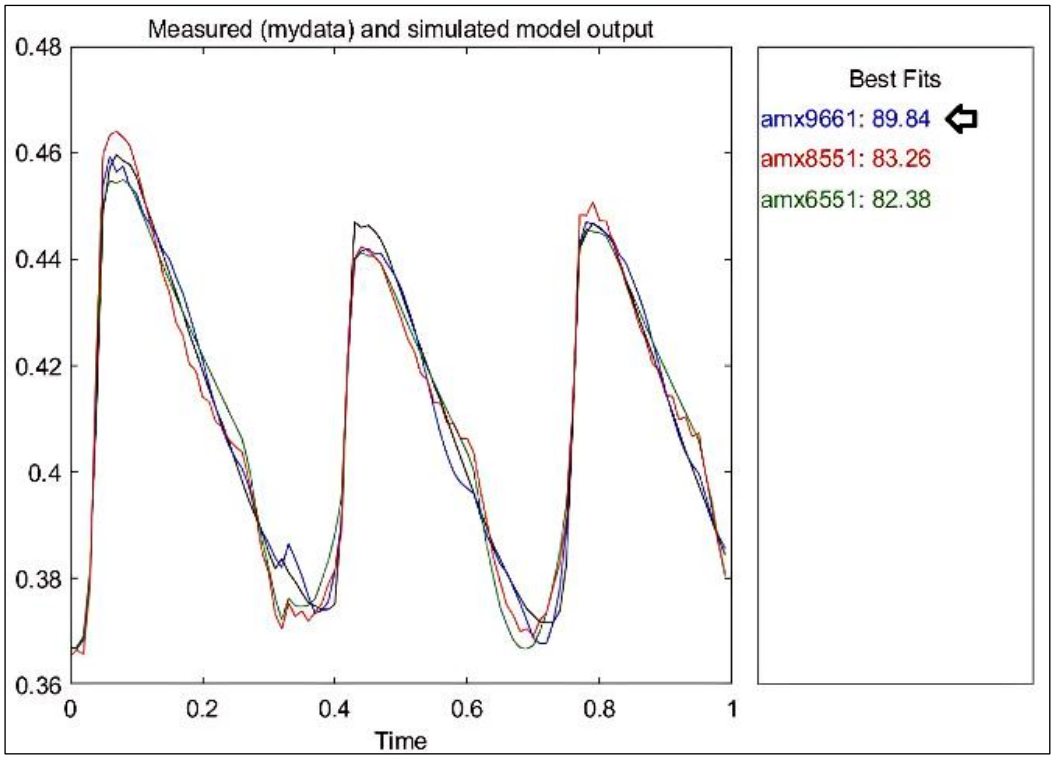

Fig. 15. Best-fit for SC's ARMAX model outputs 0.4 A

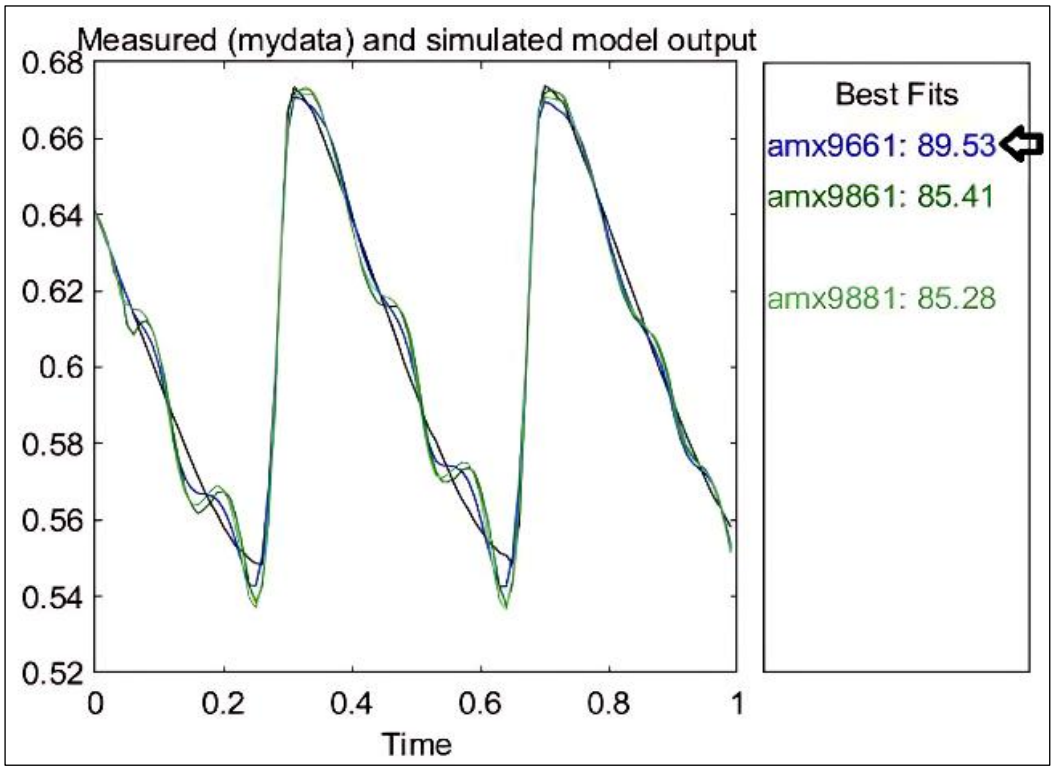

Fig. 16. Best-fit for SC's ARMAX model outputs 0.6 A

The main finding of this study is that the discharge behavior of both SCs and batteries supplying a BLDC motor can be accurately represented using control oriented mathematical models. The results show that ARMAX models consistently provide higher prediction accuracy than ARX models, indicating their stronger capability to represent system dynamics influenced by switching and load variations. More importantly, the developed models can serve as reference models for optimizing the discharge rate of energy storage systems when powering BLDC motors. By associating specific discharge current levels with defined operating speeds, the models support controlled energy delivery.

Table 4. ARX Mathematical Equation for battery and SC with parameter

Battery (0.4 A)	SC (0.6 A)
Best-fit =89.11% at (10,9,1) order $A(z)y(t) = B(z)u(t) + e(t)$ $A(z) = 1 - 1.536z^{-1} + 1.481z^{-2} - 0.9278z^{-3} + 0.4543z^{-4} + 0.1877z^{-5} - 0.6036z^{-6} + 0.093z^{-} + 0.9888z^{-8} - 0.3763z^{-9} - 0.7258z^{-10}$ $B(z) = 0.0002719z^{-1} - 0.0001434z^{-2} - 0.0004292z^{-} + 0.0002583z^{-4} + 0.0004475z^{-5} + 0.0001268z^{-} - 3.059e^{-05}z^{-7} + 5.499e^{-05}z^{-8} + 4.732e^{-05}z^{-9}$	Best-fit = 86.26% at (10,10,1) order $A(z)y(t) = B(z)u(t) + e(t)$ $A(z) = 1 - 2.011z^{-1} + 1.372z^{-2} - 0.1048z^{-3} - 0.2558z^{-4} + 0.1518z^{-5} - 0.1412z^{-6} + 0.6194z^{-7} - 0.4129z^{-8} - 0.3677z^{-9} + 0.1605z^{-10}$ $B(z) = -9.043e^{-05}z^{-1} + 0.0003819z^{-2} - 0.0002872z^{-3} + 2.36e^{-05}z^{-4} - 0.0001304z^{-5} + 0.0001508z^{-6} - 0.00029z^{-7} + 7.136e^{-05}z^{-8} + 8.89e^{-05}z^{-9} + 0.0002698z^{-10}$

Table 5. ARMAX Mathematical Equation for battery and SC with parameter

Battery (0.4 A)	SC (0.4 A)
Best-fit = 91.96% at (10,8,8,1) order $A(z)y(t) = B(z)u(t) + C(z)e(t)$ $A(z) = 1 - 2.335z^{-1} + 1.44z^{-2} + 0.5633z^{-3} - 0.3551z^{-4} - 1.053z^{-5} + 1.341z^{-6} - 0.70425z^{-7} + 0.04111z^{-8} + 0.08954z^{-9} - 0.02515z^{-10}$ $B(z) = -0.000467z^{-1} + 0.001288z^{-2} - 0.0009596z^{-3} - 0.0002476z^{-4} - 0.0003148z^{-5} + 0.0004427z^{-6} - 0.0005859z^{-7} + 0.0002726z^{-8}$ $C(z) = 1 - 0.8975z^{-1} + 0.2054z^{-2} - 0.2632z^{-3} - 0.007795z^{-4} - 0.1491z^{-5} + 0.1904z^{-6} - 0.05254z^{-7} + 0.3049z^{-8}$	Best-fit = 89.84% at (9,6,6,1) order $A(z)y(t) = B(z)u(t) + C(z)e(t)$ $A(z) = 1 - 1.82z^{-1} + 0.1737z^{-2} + 1.11z^{-3} + 0.1019z^{-4} - 0.713z^{-5} + 0.2332z^{-6} - 0.1588z^{-7} + 0.08015z^{-8} - 0.003194z^{-9}$ $B(z) = -0.0004292z^{-1} + 0.0008667z^{-2} - 6.758e^{-05}z^{-3} - 0.0006112z^{-4} - 4.272e^{-05}z^{-5} + 0.0003341z^{-6}$ $C(z) = 1 - 0.7776z^{-1} - 0.7062z^{-2} + 0.08669z^{-3} + 0.7832z^{-4} - 0.2742z^{-5} + 0.06512z^{-6}$

4. Conclusion

This study successfully obtained ARX and ARMAX models that could explain steady-state discharge behaviors of batteries and supercapacitors for a closed-loop BLDC motor drive. The ARMAX model had the highest fit of up to 91.96%, better than ARX models by approximately 3%. These findings confirm the validity of the use of ARMAX for realistic ESS modeling for real-time EV implimentation although the experimental is limited to the lab scale without real driving EV application. Practically, this improvement directly contributes to more stable current regulation and improved disturbance rejection, which are essential for reliable energy management in BLDC-driven EV systems. Moreover, this improvement also enhances system control performance by enabling more accurate current regulation through a universal modelling approach that can be applied at specific motor operating speeds. By designing models corresponding to defined reference currents, the controller can achieve reliable and consistent performance adapting to different speed regions. The limitation of the proposed approach lies in its operating-point dependency. The identified models are valid for specific speed conditions, represented by reference currents of 0.4 A for low-speed operation and 0.6 A for higher-speed operation. Behaviour outside these operating regions, including wide speed variation and fast transients, is not fully captured. Future research will extend modeling to nonlinear NARX/NARMAX structures under transient regenerative braking and load profiles, integrating adaptive control for real-time energy optimization.

Author Contribution: All authors contributed equally to the main contributor to this paper. All authors read and approved the final paper.

Funding: This research received no external funding.

Acknowledgment: The authors gratefully acknowledge the support, research facilities and publication funding provided by Universiti Malaysia Perlis (UNIMAP) and the International Islamic University Malaysia (IIUM), with additional funding and assistance from the Ministry of Higher Education (MOHE) of Malaysia.

Conflicts of Interest: The authors declare no conflict of interest.

References

[1] S. A. Razak and E. Normanyo, "Modelling and Simulation of an Electric Motor-Generator Set for Internal Combustion Engine Replacement," *Application of Modelling and Simulation journal*, vol. 5, pp. 134–144, 2021, https://arqiipubl.com/ojs/index.php/AMS_Journal/article/view/271/119.

[2] Z. B. Abdullah, S. W. Shneen, and H. S. Dakheel, "Performance Enhancement of BLDC Motor Drive Systems Using Fuzzy Logic Control and PID Controller for Improved Transient Response and Stability," *International Journal of Robotics and Control Systems*, vol. 5, no. 2, pp. 1552–1570, 2025, https://doi.org/10.31763/ijrcs.v5i2.1882.

[3] Z. A. Al-Dabbagh and S. W. Shneen, "Design of a PID Speed Controller for BLDC Motor with Cascaded Boost Converter for High-Efficiency Industrial Applications," *International Journal of Robotics and Control Systems*, vol. 5, no. 1, pp. 22–46, 2025, https://doi.org/10.31763/ijrcs.v5i1.1601.

[4] B. Ramesh, K. Chenchireddy, B. N. Reddy, B. Siddharth, C. V. Kumar, and P. Manojkumar, "Closed-loop control of BLDC motor using Hall effect sensors," *International Journal of Applied Power Engineering*, vol. 12, no. 3, pp. 247–254, 2023, https://doi.org/10.11591/ijape.v12.i3.pp247-254.

[5] A. Hasni, H. Fadil, A. Lassioui, M. Ancary, Y. El Asri, A. Hamed, and S. El Jeilani "Optimized Speed Regulation of BLDC Motors: A Comparative Performance Study of Artificial Neural Networks and Super-Twisting Sliding Mode Controllers," *International Journal of Robotics and Control Systems*, vol. 5, no. 4, pp. 2360–2378, 2025, https://pubs2.ascee.org/index.php/IJRCS/article/view/2046.

[6] G. A. Aziz, F. N. Abdullah, and S. W. Shneen, "Performance Enhancement of DC Motor Drive Systems Using Genetic Algorithm-Optimized PID Controller for Improved Transient Response and Stability," *International Journal of Robotics and Control Systems*, vol. 5, no. 1, pp. 266–295, 2025, https://doi.org/10.31763/ijrcs.v5i1.1602.

[7] E. Boloor Kashani and A. Halvaei Niasar, "Reduction of torque ripple in an electrolytic capacitor-less BLDC motor drive by simultaneous speed and torque control method," *Ain Shams Engineering Journal*, vol. 12, no. 4, pp. 3703–3709, 2021, https://doi.org/10.1016/j.asej.2020.12.021.

[8] H. Masoudi, A. Kiyoumarsi, S. M. Madani, and M. Ataei, "Closed-Loop Direct Power Control of Brushless DC Motor in Field Weakening Region," *IEEE Transactions on Transportation Electrification*, vol. 10, no. 2, pp. 3482–3491, 2024, https://doi.org/10.1109/TTE.2023.3305050.

[9] Y. P. Shen, J. C. Xie, X. F. Yuan, S. N. Sun, and H. M. Du, "Power Distribution Strategy of Fourth-level Haar Wavelet for Hybrid Energy Storage Systems in Electric Vehicle," *Journal of Electrical Engineering and Technology*, vol. 20, no. 3, pp. 1485–1496, 2025, https://doi.org/10.1007/s42835-024-02067-4.

[10] C. V. M. Gopi and R. Ramesh, "Review of battery-supercapacitor hybrid energy storage systems for electric vehicles," *Results in Engineering*, vol. 24, p. 103598, 2024, https://doi.org/10.1016/j.rineng.2024.103598.

[11] A. A. Rizi, A. Rezaei, M. G. Rizi, and M. A. Rizi, "Design a New Multiport DC-DC Converter to Charge an Electric Car," *International Journal of Robotics and Control Systems*, vol. 2, no. 1, pp. 87–96, 2022, https://doi.org/10.31763/ijrcs.v2i1.566.

[12] A. T. Hamada and M. F. Orhan, "An overview of regenerative braking systems," *Journal of Energy Storage*, vol. 52, p. 105033, 2022, https://doi.org/10.1016/j.est.2022.105033.

[13] N. Hannan, S. K. Shib, A. Shufian, M. A. Islam, S. M. Islam Sharan, and A. Das Gupta, "Advanced regenerative braking system for EVs: Leveraging BLDC-supercapacitor technologies for optimized

energy recovery, economic viability, and maintenance strategies," *Future Batteries*, vol. 7, p. 100103, 2025, https://doi.org/10.1016/j.fub.2025.100103.

[14] L. Yang, X. Wang, B. Jin, Y. Gao, and H. Zhang, "Efficiency Improvement for Regenerative Energy System Using Dynamic Efficiency-SOC-Load Model," *Journal of Electrical Engineering and Technology*, vol. 18, no. 1, pp. 419–429, 2023, https://doi.org/10.1007/s42835-022-01115-1.

[15] C. Yang, T. Sun, W. Wang, Y. Li, Y. Zhang, and M. Zha, "Regenerative braking system development and perspectives for electric vehicles: An overview," *Renewable and Sustainable Energy Reviews*, vol. 198, p. 114389, 2024, https://doi.org/10.1016/j.rser.2024.114389.

[16] V. Kumar, K. Chenchireddy, K. R. Sreejyothi, and G. Sujatha, "Design and Development of Brushless DC Motor Drive for Electrical Vehicle Application," *AI Enabled IoT for Electrification and Connected Transportation*, pp. 201–217, 2022, https://doi.org/10.1007/978-981-19-2184-1_10.

[17] J. Cureño-Osornio, C. Alvarez-Ugalde, I.Zamudio-Ramirez, R. Osornio-Rios, L. Dunai, D. Turcanu, and J. Antonino-Daviu, "Start-Up and Steady-State Regimes Automatic Separation in Induction Motors by Means of Short-Time Statistics," *Electronics*, vol. 13, no. 19, 2024, https://doi.org/10.3390/electronics13193850.

[18] B. Benbouya, H. Cheghib, M. Behim, M. Mahmoud, M. Elnaggar, N. Ibrahim, and N. Anwer, "Dynamic Assessment and Control of a Dual Star Induction Machine State Dedicated to an Electric Vehicle Under Short-Circuit Defect," *International Journal of Robotics and Control Systems*, vol. 4, no. 4, pp. 1731–1745, 2024, https://doi.org/10.31763/ijrcs.v4i4.1557.

[19] M. A. El Sawy, O. M. Kamel, Y. S. Mohamed, and M. A. Mossa, "Dynamic Performance Evaluation of a Brushless AC Motor Drive Using Different Sensorless Schemes," *International Journal of Robotics and Control Systems*, vol. 4, no. 2, pp. 502–535, 2024, https://doi.org/10.31763/ijrcs.v4i2.1306.

[20] Q.-C. Nguyen, V.-H. Vu, and M. Thomas, "Optimal ARMAX Model Order Identification of Dynamic Systems," *London Journal of Engineering Research*, vol. 22, no. 1, pp. 1–22, 2022, https://journalspress.uk/index.php/LJER/article/view/407.

[21] B. Ale, "Modeling and Performance Analysis of an In-wheel Permanent Magnet Brushless DC (PM BLDC) Motor in MATLAB," *Application of Modelling and Simulation*, vol. 6, no. 6, pp. 150–157, 2022, https://arqiipubl.com/ojs/index.php/AMS_Journal/article/view/372.

[22] B. Tian and H. Peng, "A fast robust output tracking approach based on the GRU-ARX model with application to quadrotor," *Applied Mathematical Modelling*, vol. 151, 2026, https://doi.org/10.1016/j.apm.2025.116429.

[23] Y. Yang, "Data-driven RTO and computationally efficient MPC using piecewise ARX models for unknown process dynamics," *Computers & Chemical Engineering*, vol. 204, 2026, https://doi.org/10.1016/j.compchemeng.2025.109423.

[24] X. Zhang, D. Saelens, and S. Roels, "Estimating dynamic solar gains from on-site measured data: An ARX modelling approach," *Applied Energy*, vol. 321, 2022, https://doi.org/10.1016/j.apenergy.2022.119278.

[25] R. A. P. Franco, Á. A. Cardoso, G. L. Filho, and F. H. T. Vieira, "MIMO auto-regressive modeling-based generalized predictive control for grid-connected hybrid systems," *Computers and Electrical Engineering*, vol. 97, 2022, https://doi.org/10.1016/j.compeleceng.2021.107636.

[26] Q. C. Nguyen, V. H. Vu, and M. Thomas, "A Kalman filter based ARX time series modeling for force identification on flexible manipulators," *Mechanical Systems and Signal Processing*, vol. 169, 2022, https://doi.org/10.1016/j.ymssp.2021.108743.

[27] V. De Iuliis, F. Smarra, C. Manes, and A. D'Innocenzo, "Stability analysis of switched ARX models and application to learning with guarantees," *Nonlinear Analysis: Hybrid Systems*, vol. 46, 2022, https://doi.org/10.1016/j.nahs.2022.101250.

[28] J. Tomperi, A. Sorsa, J. Ruuska, and M. Ruusunen, "Series-connected data-based model to estimate effluent chemical oxygen demand in industrial wastewater treatment process," *Journal of Environmental Management*, vol. 373, 2025, https://doi.org/10.1016/j.jenvman.2024.123680.

[29] V. L. G. da Silva, D. O. Filho, J. C. Carlo, and P. N. Vaz, "An Approach to Solar Radiation Prediction Using ARX and ARMAX Models," *Frontiers in Energy Research*, vol. 10, 2022, https://doi.org/10.3389/fenrg.2022.822555.

[30] H. Maghfiroh, A. J. Titus, A. Sujono, F. Adriyanto, and J. S. Saputro, "Induction Motor Torque Measurement using Prony Brake System and Close-loop Speed Control," *International Journal of Robotics and Control Systems*, vol. 2, no. 3, pp. 594–605, 2022, https://doi.org/10.31763/ijrcs.v2i3.782.

[31] S. Amosedinakaran, M. Mano Raja Paul, S. Kannan, M. Geetha, P. Anitha, and A. Bhuvanesh, "Performance analysis of battery E-vehicle system using open loop and closed loop application," *Measurement: Sensors*, vol. 31, 2024, https://doi.org/10.1016/j.measen.2023.100963.

[32] P. M. Krishna and T. Srinu, "Analysis of Closed Loop Current Controlled BLDC Motor Drive," *International Journal of Scientific Research in Engineering and Management*, vol. 8, no. 6, pp. 1–5, 2024, https://doi.org/10.55041/IJSREM35689.

[33] H. Fu, Z. Ma, A. Liu, and L. Sun, "Dynamic modeling and model predictive control of a nonlinear time-varying closed-loop heat pump drying system with exhaust heat recovery," *Applied Thermal Engineering*, vol. 280, 2025, https://doi.org/10.1016/j.applthermaleng.2025.127980.

[34] Y. Fan, Q. Zhao, C. Wan, and J. Shi, "Closed-loop co-simulation of indirect air-cooling system for improved prediction of thermal performance," *Applied Thermal Engineering*, vol. 280, 2025, https://doi.org/10.1016/j.applthermaleng.2025.128528.

[35] D. Yang, J. Wang, N. Ban, Y. Zhong, D. Wong, A. Razminia, and C. Cui, "Model predictive control of pressure-swing distillation via closed-loop system identification," *Journal of Process Control*, vol. 156, p. 103589, Dec. 2025, https://doi.org/10.1016/j.jprocont.2025.103589.

[36] A. Singh, K. Pal, and C. B. Vishwakarma, "State of charge estimation techniques of Li-ion battery of electric vehicles," *e-Prime - Advances in Electrical Engineering, Electronics and Energy*, vol. 6, 2023, https://doi.org/10.1016/j.prime.2023.100328.

[37] M. Z. Afzal, F. Wen, N. Saeed, and M. Aurangzeb, "Enhanced state of charge estimation in electric vehicle batteries using chicken swarm optimization with open ended learning," *Scientific Reports*, vol. 15, no. 1, 2025, https://doi.org/10.1038/s41598-025-90374-9.

[38] N. T. Diep and N. K. Trung, "An online battery–state of charge estimation method using the varying forgetting factor recursive least square-unscented Kalman filter algorithm on electric vehicles," *International Journal of Electrical and Computer Engineering*, vol. 14, no. 3, pp. 2541–2553, 2024, https://doi.org/10.11591/ijece.v14i3.pp2541-2553.

[39] S. Bouzaid, L. El Mehdi, and A. El Ballouti, "A fast charge algorithm for Li-ion battery for electric vehicles," *International Journal of Electrical and Computer Engineering*, vol. 14, no. 3, pp. 2457–2465, 2024, https://doi.org/10.11591/ijece.v14i3.pp2457-2465.

[40] M. K. Baek, J. H. Roh, J. B. Park, and W. C. Jeong, "Optimal Sizing of Battery/Supercapacitor Hybrid Energy Storage Systems for Frequency Regulation," *Journal of Electrical Engineering and Technology*, vol. 17, no. 1, pp. 111–120, 2022, https://doi.org/10.1007/s42835-021-00867-6.

[41] Z. Bin Zhu, S. M. Sun, Y. M. Ding, and S. P. Huang, "Research on Control Strategy of Hybrid Energy Storage System with Optical Storage Microgrid," *Journal of Electrical Engineering and Technology*, vol. 18, no. 4, pp. 2835–2845, 2023, https://doi.org/10.1007/s42835-022-01367-x.

[42] Z. Bououchma and A. El, "User-centered optimization of hybrid battery/supercapacitor storage systems in electric vehicles," *FME Transactions*, vol. 53, no. 4, pp. 575–584, 2025, https://doi.org/10.5937/fme2504575B.

[43] Jumiyatun, M. Ashari, Soedibyo, and H. Suryoatmojo, "Optimal Supercapacitor Size to Enhance Battery Life Under Large Intermittent Load Variations," *International Journal on Engineering Applications*, vol. 12, no. 5, pp. 347–356, 2024, https://doi.org/10.15866/irea.v12i5.24759.

[44] M. Mossaddek, E. M. Laadissi, C. Ennawaoui, S. Bouzaid, and A. Hajjaji, "Enhancing battery system identification: nonlinear autoregressive modeling for Li-ion batteries," *International Journal of Electrical and Computer Engineering*, vol. 14, no. 3, pp. 2449–2456, 2024, https://doi.org/10.11591/ijece.v14i3.pp2449-2456.

[45] P. Roja, D. Venkatramanan, and V. John, "A Nonlinear Model Based Analysis and Accurate Design of Ultracapacitor Stack for Energy Storage Systems," *IEEE Transactions on Energy Conversion*, vol. 37, no. 1, pp. 403–412, 2022, https://doi.org/10.1109/TEC.2021.3086019.

[46] M. Haidoury, M. Rachidi, H. El Hadraoui, O. Laayati, Z. Kourab, S. Tayane, and M. Ennaji, "Hybrid fuel cell-supercapacitor system: Modeling and energy management using Proteus," *International Journal of Electrical and Computer Engineering*, vol. 14, no. 1, pp. 110–128, 2024, https://doi.org/10.11591/ijece.v14i1.pp110-128.

[47] M. A. Mossa, O. Gam, and N. Bianchi, "Performance Enhancement of a Hybrid Renewable Energy System Accompanied with Energy Storage Unit Using Effective Control System," *International Journal of Robotics and Control Systems*, vol. 2, no. 1, pp. 140–171, 2022, https://doi.org/10.31763/ijrcs.v2i1.599.

[48] J. K. Chavda, S. Prajapati, R. Babariya, C. Vibhakar, N. Patel, and V. A. Shah, "Hybrid Energy Management System Consisting of Battery and Supercapacitor for Electric Vehicle," *International Journal of Integrated Engineering*, vol. 14, no. 7, pp. 94–107, 2022, https://doi.org/10.30880/ijie.2022.14.07.008.

[49] Q. S. Wei, X. Zhang, B. H. Kim, and B. S. Oh, "Experimental investigation of supercapacitor based regenerative energy storage for a fuel cell vehicle equipped with an alternator," *International Journal of Hydrogen Energy*, vol. 47, no. 3, pp. 1954–1964, 2022, https://doi.org/10.1016/j.ijhydene.2021.10.102.

[50] P. Vankadari, "Comparison Study of Battery & Supercapacitor Standalone Storage System Based Light Electric Vehicle Using MATLAB/SIMULINK," *International Journal for Research in Applied Science and Engineering Technology*, vol. 9, no. 12, pp. 1071–1082, 2021, https://doi.org/10.22214/ijraset.2021.39471.

[51] M. S. Ramkumar, S. Muthukrishnan, J. Giri, T. Sathish, and A. Fatehmulla, "Optimizing battery and supercapacitor management in electric vehicles: A hybrid approach for enhanced performance and reduced harmonics," *Case Studies in Thermal Engineering*, vol. 68, 2025, https://doi.org/10.1016/j.csite.2025.105815.

[52] M. Dasari, A. Srinivasula Reddy, and M. Vijaya Kumar, "A comparative analysis of converters performance using various control techniques to minimize the torque ripple in BLDC drive system," *Sustainable Computing: Informatics and Systems*, vol. 33, pp. 1–14, 2022, https://doi.org/10.1016/j.suscom.2021.100648.

[53] R. K. Gaber, S. W. Shneen, and S. M. Jiaad, "Study and Analysis of PWM with DC-DC Converter for Inverting Buck-Boost Inverter Topology," *International Journal of Robotics and Control Systems*, vol. 5, no. 2, pp. 1029–1050, 2025, https://doi.org/10.31763/ijrcs.v5i2.1823.

[54] O. J. Tola, E. A. Umoh, and E. A. Yahaya, "Pulse Width Modulation Analysis of Five-Level Inverter-Fed Permanent Magnet Synchronous Motors for Electric Vehicle Applications," *International Journal of Robotics and Control Systems*, vol. 1, no. 4, pp. 477–487, 2021, https://doi.org/10.31763/ijrcs.v1i4.483.

[55] Ayushjain, "DC-DC Converter Efficiency: Why It Matters and How to Maximize It - The Law Brigade Publishers (India)," *The Law Brigade Publisher*, 2025, https://thelawbrigade.com/general-research/dc-dc-converter-efficiency-why-it-matters-and-how-to-maximize-it/.

[56] N. Ratnawati and S. Sunardi, "Load Characteristics with Current Detection Using an Arduino Based ACS712 Sensor," *Buletin Ilmiah Sarjana Teknik Elektro*, vol. 2, no. 2, p. 83, 2020, https://doi.org/10.12928/biste.v2i2.1522.

[57] Engineers Garage Projects, "How to measure current using Arduino and ACS712 current sensor," *www.engineersgarage.com*, www.engineersgarage.com.

[58] T. Yuan, J. Chang, and Y. Zhang, "Research on the Current Control Strategy of a Brushless DC Motor Utilizing Infinite Mixed Sensitivity Norm," *Electronics*, vol. 12, no. 21, 2023, https://doi.org/10.3390/electronics12214525.

[59] A. M. Caiza, E. F. M. Garces, G. Mafla, J. Guerra, and W. Villalba, "Identification of dynamical systems through the structure of auto-regression with exogenous variable by decreasing gradient and least squares," *WSEAS Transactions on Mathematics*, vol. 20, pp. 676–682, 2021, https://doi.org/10.37394/23206.2021.20.71.

[60] L. K. Fong, M. S. Islam, and M. A. Ahmad, "Optimized PID Controller of DC-DC Buck Converter based on Archimedes Optimization Algorithm," *International Journal of Robotics and Control Systems*, vol. 3, no. 4, pp. 658–672, 2023, https://doi.org/10.31763/ijrcs.v3i4.1113.

[61] Z. Cabrane and S. H. Lee, "Electrical and Mathematical Modeling of Supercapacitors: Comparison," *Energies*, vol. 15, no. 3, 2022, https://doi.org/10.3390/en15030693.